Site-Specific and Coherent Manipulation of Individual Qubits in a 1D Optical Lattice with a 532-nm Site Separation

Hyok Sang Han, Hyun Gyung Lee, and D. Cho*
Department of Physics, Korea University, Seoul 02841, Korea

(Received 5 September 2018; published 5 April 2019)

We demonstrate gate operations on a single qubit at a specific site without perturbing the coherence of an adjacent qubit in a 1D optical lattice when the site separation is only 532 nm. Three types of spin rotations are performed on the target qubit with fidelities between 0.88 ± 0.05 and 0.99 ± 0.01, whereas the superposition state of the adjacent one is preserved with fidelities between 0.93 ± 0.04 and 0.97 ± 0.04. The qubit is realized by a pair of Zeeman-sensitive ground hyperfine states of a ^{7}Li atom, and each site is identified by its resonance frequency in a magnetic field gradient of 1.6 G/cm. We achieve the site-specific resolving power in the frequency domain by using magic polarization for the lattice beam that allows a Fourier-limited transition linewidth as well as by highly stabilizing the lattice parameters and the ambient conditions. We also discuss a two-atom entanglement scheme using a blockade by cold collisional shifts in a 1D superlattice, for which a coherent manipulation of individual qubits is a prerequisite.

DOI: 10.1103/PhysRevLett.122.133201

Atoms in a 1D optical lattice, with a pair of ground hyperfine states constituting a qubit, provide one of the simplest platforms to test basic gate operations and the scalability in quantum information processing. Protocols for entangling the atomic qubits in adjacent sites via cold collisions have been proposed [1,2], and a proof-of-principle experiment was reported [3]. However, weakness of the cold collisional interaction mandates site separation a of only ~ 0.5 μm, and it makes site-specific addressing of individual qubits very difficult. Research interest has shifted to protocols that exploit the strong dipolar interaction of Rydberg atoms [4], which allows entanglement of two atoms separated by a few micrometers [5]. In spite of recent progress [6], however, the control of Rydberg qubits remains challenging because the highly excited states suffer from a dense level structure, spontaneous emission, and even interaction with blackbody radiation [7]. The ground hyperfine states, in contrast, are simple, stable, and well isolated; and the platform based on them can be complementary to or even better than the Rydberg scheme if a reliable entanglement and site-specific addressing become possible.

For entanglement, there are new ideas in addition to the original proposals. For example, using a 1D superlattice of wavelengths λ and 2λ [8], adjacent sites in a λ lattice can be merged by imposing a 2λ beam. Two atoms, thus put in the same site and further cooled to the motional ground state, can be entangled by "motional blockade" in a way analogous to the Rydberg blockade. Here, a motion-dependent collisional shift, enhanced by Feshbach resonance, plays the role of the state-dependent dipolar shift. Repeating it using a properly shifted 2λ beam may produce a cluster state for a one-way quantum computing [9,10].

To address individual qubits in a 1D lattice, which is a prerequisite for a multiqubit manipulation, a magnetic field gradient is applied to induce a site-dependent Zeeman shift [11–13]. Despite its simplicity, the method was not successful when $a \approx 0.5$ μm, mainly because an ac Stark shift from the lattice beam broadened the hyperfine transition [14]. For Cs atoms in a 433-nm lattice [12], a large gradient b of 61.5 G/cm was applied to overcome the broadening, but the nearest site was not clearly resolved. In addition, drift and noise in a magnetic field destroy site specificity, and the large gradient exacerbated these problems. On the other hand, in a 2D or 3D lattice, a laser beam is focused on a target atom to induce an ac Stark shift [15]. Although a site-specific spin flip was accomplished in a 2D lattice with $a = 532$ nm using this method [16], a site-specific spin rotation during adjacent qubits kept in a superposition state was demonstrated only in a 3D lattice with a as large as 4.9 μm [17,18].

In this Letter, we report an experiment in a 1D lattice with $a = 532$ nm to perform spin rotations of a single ^{7}Li atom at a specific site with minimum disturbance to coherence of an adjacent atom in a superposition state. We employ two strategies. (i) Elimination of the inhomogeneous broadening by using magic polarization [19]. This allows the reduction of b to 1.6 G/cm, thereby mitigating difficulties arising from the drift and noise. (ii) Tight control of experimental parameters by using a low-expansion mounting system, a three-layer magnetic shield, and a network of stabilization systems.

Slow atoms from a magneto-optical trap (MOT) enter the octagonal glass chamber as shown in Fig. 1(a). They are transferred to the lattice by the second MOT. The 1D lattice is formed along the z axis by focusing a 1064-nm beam to

the e^{-2} intensity radius of 14 μm and reflecting it back with a matching mode. When the incident power is 1.3 W, the well depth U_0 at an antinode, measured in units of the Boltzmann constant k_B, is 1 mK. The MOT lasers also serve as probe beams. Atomic fluorescence is collected by a lens with a numerical aperture (NA) of 0.22 and refocused to an electron-multiplying charge-coupled device (EMCCD) with unit magnification [20,21]. The overall detection efficiency of the fluorescence photon is 1%.

We use the $|\chi_0\rangle = |2S_{1/2}, F = 2, m_F = -2\rangle$ and $|\chi_1\rangle = |2S_{1/2}, F = 1, m_F = -1\rangle$ states of ^{7}Li as the qubit. F and m_F are the total and the z component angular momentum, respectively. Transition between them at 803 MHz is driven by a radio frequency (rf) antenna. Inhomogeneous broadening is less than 10 Hz at $U_0 = 0.7$ mK when the polarization of the lattice beam satisfies the magic condition [19]. In comparison, the difference in Zeeman shifts between adjacent sites ($\Delta f_Z = 3\mu_B ab/2h$ with μ_B being a Bohr magneton) is 180 Hz. The transition frequency f_0 at a specific site q_0, where a target atom is loaded, should be stable to a small fraction of Δf_Z during a few hours of data taking. In order to keep f_0 constant within 1 Hz, we do the following. (i) We mount both the retro-optics for the lattice and an anti-Helmholtz coil for the gradient onto a frame made of a material with a low thermal expansion (Zerodur). (ii) To keep a constant, the lattice-beam frequency is locked to a cavity for which the length is stabilized to the 852-nm Cs transition. (iii) A three-layer magnetic shield with a shielding factor of 10^6 encloses the chamber. (iv) The current through a Helmholtz coil, which provides 0.4 G of quantization field $B_0\hat{z}$, is stabilized to 10^{-6}. (v) The lattice and gradient field are aligned, both longitudinally and transversely, such that a drift in field slope would not affect f_0 to the first order.

We start experiments by loading and Doppler cooling atoms in the optical lattice at $U_0 = 2.1$ mK. Each site is occupied by either one or no atoms owing to pairwise photoassociative escapes. We first measure the distribution of atoms by performing rf spectroscopy in a B field gradient. Atoms are optically pumped to $|\chi_0\rangle$ under $B_0\hat{z}$ using the $D1$ transitions. Less than 10^{-4} of atoms are left in states other than $|\chi_0\rangle$. Such a high efficiency is important to minimize the sample preparation and measurement error in gate operations. We then turn on $b = 1.6$ G/cm and apply an rf field to drive a site-selective transition to $|\chi_1\rangle$. The rf is enveloped by a Blackman window of 20 ms duration, yielding a full width at half-maximum of 75 Hz as compared with $\Delta f_Z = 180$ Hz. When transferred to a magnetic trap, only an atom that has undergone a transition to $|\chi_1\rangle$ remains trapped, and its MOT fluorescence is detected by the EMCCD with single-atom precision [20]. Such a detection results in either one or no atoms. The histogram in Fig. 1(b) shows the number of one-atom detections out of 20 trials as we scan the rf frequency across the resonances of three sites. Consecutive sites, labeled

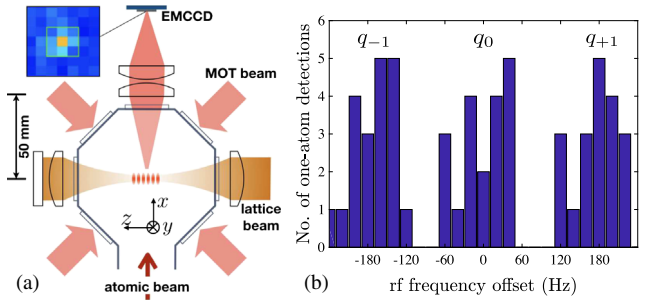

FIG. 1. (a) Octagonal glass chamber and optics to trap and image atoms. (b) Number of one-atom detections out of 20 trials vs rf frequency offset. Three consecutive sites (labeled q_{-1}, q_0, and q_{+1}) are clearly resolved.

q_{-1}, q_0, and q_{+1}, are clearly resolved. The histogram is reminiscent of atom images in the spatial domain obtained by high-NA systems [22,23], in which the diffraction limit δz is reduced below the site separation a. We achieve essentially the same feat in the frequency domain by reducing the transition linewidth δf below the Zeeman shift per site Δf_Z.

The above method using a magnetic trap and a MOT allows state-selective removal ($|\chi_0\rangle$) and detection ($|\chi_1\rangle$) with near-100% efficiency. However, it is destructive. In order to keep the target atom that has made a transition to $|\chi_1\rangle$ intact for subsequent *in situ* manipulation, we selectively push out the atoms in $|\chi_0\rangle$. We lower U_0 to 0.1 mK, and we push atoms along the less stiff transverse axis of the lattice. $B_0\hat{z}$ is rotated to $B_0\hat{x}$, and a left-circularly polarized beam, tuned to the $|\chi_0\rangle \to |2P_{3/2}, F = 3, m_F = -3\rangle$ transition at the saturation intensity, is applied for 30 μs. Ninety-seven percent of $|\chi_0\rangle$ atoms are removed, and almost no $|\chi_1\rangle$ atoms are lost. The remaining 3% of $|\chi_0\rangle$ atoms are in the wrong sites, and they can significantly complicate the analysis of target-atom gate operations. We repeat the cycle of optical pumping, rf pulse, and pushout three times to reduce the remaining fraction below 3×10^{-5}. After the iteration with the rf tuned to f_0, a fluorescence image is taken to determine whether a single atom is left in the lattice. When illuminated by a probe beam, however, a Li atom tends to boil out because of large recoil energy and poor sub-Doppler cooling. A sideband-cooling stage was necessary for its *in situ* imaging [24]. We simply use a deep well ($U_0 = 2.1$ mK) that can hold atoms for 1 min with only the Doppler cooling from the probe beam itself [21].

After the three iterations, we find a single atom with 40% probability. It cannot exceed 50% owing to the initial modulo-one distribution. We next perform Rabi and Ramsey spectroscopy of the single atom in the magnetic field gradient to demonstrate site-specific single-qubit operations. U_0 is set back to 0.7 mK. Traces in Fig. 2 are the Rabi line shapes for the single atoms loaded to the q_{-1}, q_0, and q_{+1} sites, respectively. After a 20-ms

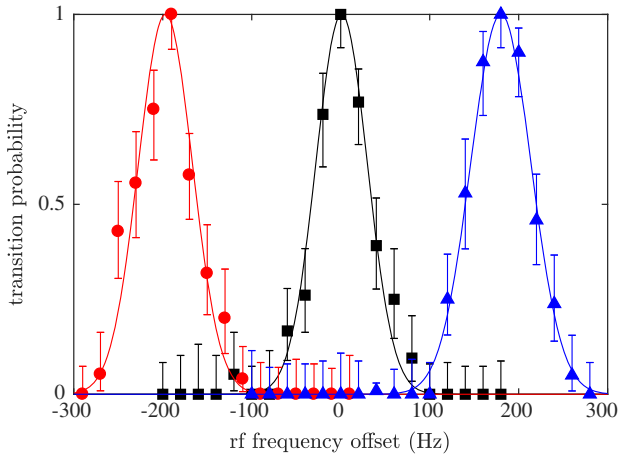

FIG. 2. Rabi line shapes for single atoms residing at the q_{-1} (red circle), q_0 (black square), and q_{+1} sites (blue triangle). Magnetic field gradient is 1.6 G/cm. Solid curves are theory predictions for a π pulse driven by a 20-ms Blackman window. The probability of unwanted transition of an atom at a nearby site is less than 0.02 at the 68% confidence level.

Blackman π pulse, transition to the $|\chi_1\rangle$ state is measured by transfer to a magnetic trap. Each data point combines 20 measurements, or ~50 loading trials, and the error bars represent the Clopper-Pearson interval at the 68% confidence level. From the data, we estimate the transition probability at the $q_{\pm1}$ site, when the rf is tuned to q_0, to be less than 0.02. This sets the upper limit on crosstalk between adjacent atoms via the π pulse. Figure 3 shows a single-atom Ramsey fringe from two consecutive 10-ms $\pi/2$ pulses with a phase offset $\Delta\phi$. If we attribute the deviation from theory (solid curve) to a drift in f_0, it is less than 0.4 Hz, or less than 0.2 μG in terms of the magnetic field, during 1 h of data taking.

The result in Fig. 2 shows a spin flip at the q_0 site without concomitant flips at $q_{\pm1}$. We extend this site-specific spin

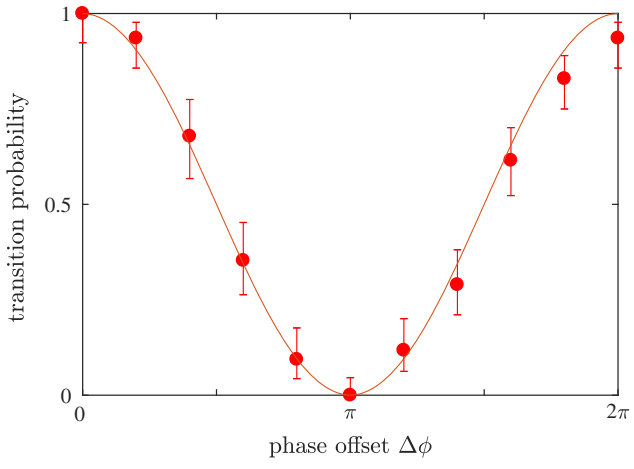

FIG. 3. Ramsey signal of a single atom vs phase offset $\Delta\phi$ between two $\pi/2$ pulses. Solid curve is a theory prediction for two consecutive 10-ms Blackman pulses.

flip to coherent gate operations by performing a few spin rotations at q_0 without disturbing coherence of the $q_{\pm1}$ qubits prepared in a superposition state. We consider three cases [17] of $R(\hat{x},\pi)$, $R(\hat{x},\pi/2)$, and $R(\hat{u},\pi)$, where $R(\hat{v},\theta)$ is a rotation about $\hat{v}$ by an angle θ and $\hat{u}=(\hat{x}+\hat{y})/\sqrt{2}$. Each rotation is preceded by a $\pi/2$ pulse of 0.1-ms duration tuned to q_0. The pulse is short enough to put both the q_0 and $q_{\pm1}$ qubits to the $|\chi_-\rangle=(|\chi_0\rangle-i|\chi_1\rangle)/\sqrt{2}$ state. Our aim is to transform the q_0 qubit to $R(\hat{v},\theta)|\chi_-\rangle$ while leaving the adjacent ones in $|\chi_-\rangle$. The spin state after the rotation is analyzed by another $\pi/2$ pulse with a phase offset $\Delta\phi$. Although the effects of each short $\pi/2$ pulse on the q_0 and $q_{\pm1}$ qubits are almost the same, application of two $\pi/2$ pulses separated by T produces a phase shift of $\pm2\pi\Delta f_Z T$ in the Ramsey signal of the $q_{\pm1}$ qubits, even without an intervening rotation $R(\hat{v},\theta)$. We remedy this situation by applying a 0.2-ms π pulse between them for a spin echo. In order to accommodate the echo pulse, $R(\hat{v},\theta)$ is split into $R(\hat{v},\theta/2)$ and $R(\hat{v}',\theta/2)$, where $\hat{v}'$ is obtained by rotating $\hat{v}$ about the x axis by π. For example, $\hat{u}'=(\hat{x}-\hat{y})/\sqrt{2}$. For the target qubit, the result of a rotation including the spin echo is $R(\hat{v}',\theta/2)R(\hat{x},\pi)R(\hat{v},\theta/2)|\chi_-\rangle$, which is equivalent to $R(\hat{x},\pi)R(\hat{v},\theta)|\chi_-\rangle$. For the nontarget qubit, which is supposed to be immune to $R(\hat{v},\theta)$, it should be simply $R(\hat{x},\pi)|\chi_-\rangle$. Figure 4(a) shows the pulse sequence. In practice, the gate operations are implemented by an rf field $\mathcal{B}(t)=a(t)\mathcal{B}_0\cos(2\pi f_0 t+\phi_p)$. Our rf system, consisting of direct digital synthesizers, mixers, and various transducers, allows us to dynamically control the envelope $a(t)$, the amplitude $|\mathcal{B}_0|$, and the phase ϕ_p. After the pulse sequence, projection to the $|\chi_1\rangle$ state is measured.

While fidlelity of the $R(\hat{v},\theta)$ operations on the q_0 qubit is limited only by technical factors such as a magnetic field drift or an rf field error, coherence of the $q_{\pm1}$ qubits may suffer from unintended perturbation by $R(\hat{v},\theta)$ as well. One of the perturbations is an ac Zeeman shift $|\Omega(t)|^2/8\pi\Delta f_Z$, where $\Omega(t)$ is a Rabi frequency from $\mathcal{B}(t)$. However, because $R(\hat{v},\theta)$ is split symmetrically with respect to the echo pulse, spin precession of approximately 0.1 rad from the shift is eliminated very well. More problematic is an off-resonant spin rotation induced by $R(\hat{v},\theta)$. By using numerical simulations, we find an optimal waveform that minimizes the rotation of $q_{\pm1}$ while maintaining a proper linewidth for the q_0 resonance. For each half-rotation in Fig. 4(a), we use an envelope $a(t)=\sin^2(\pi t/t_p)$ with $t_p=5.7$ ms for $R(\hat{x},\pi)$ and $R(\hat{x},\pi/2)$, and $t_p=9.5$ ms for $R(\hat{u},\pi)$. The simulation predicts that the probability for an unintended transition of the $q_{\pm1}$ qubits at $\Delta\phi=0$ is less than 1.5×10^{-4}.

Results of the three rotations $R(\hat{x},\pi)$, $R(\hat{x},\pi/2)$, and $R(\hat{u},\pi)$ on the q_0 (red circle) and q_{+1} (black square) qubits are shown in Figs. 4(b)–4(d), respectively. The solid curves are the intended results. In this experiment, we are not interested in direct interaction between adjacent atoms for

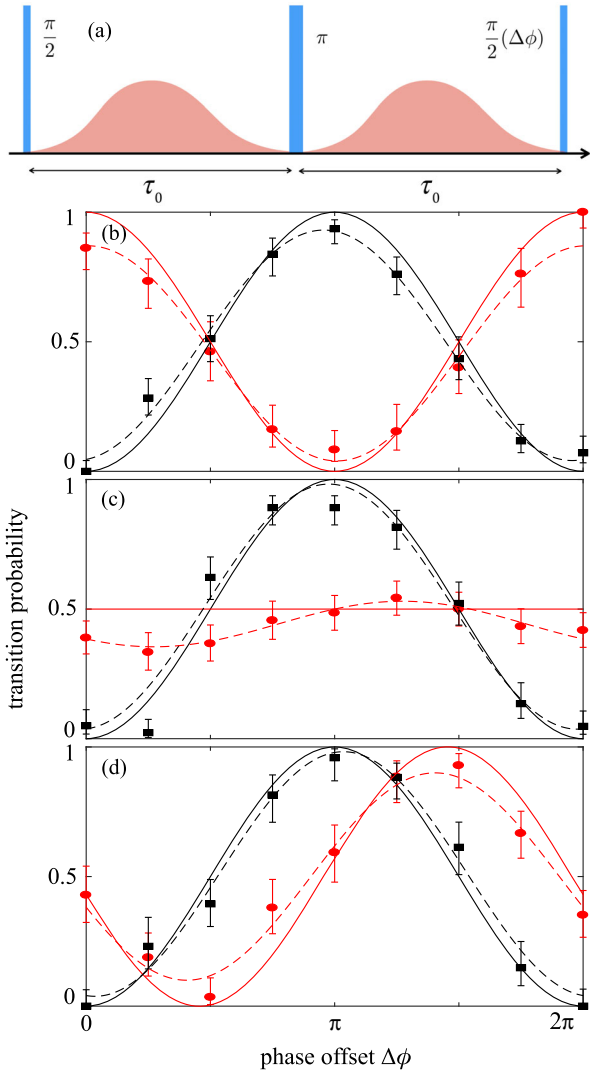

FIG. 4. (a) Pulse sequence consisting of a $\pi/2$ pulse, the first part $R(\hat{v},\theta/2)$ of a spin rotation, a π pulse for a spin echo, the second part $R(\hat{v}',\theta/2)$ of a spin rotation, and a final $\pi/2$ pulse with a phase offset $\Delta\phi$. Results of the pulse sequence on the target qubit (red circle) and the adjacent qubit (black square) for the spin rotations are shown for (b) $R(\hat{x},\pi)$, (c) $R(\hat{x},\pi/2)$, and (d) $R(\hat{u},\pi)$, where $\hat{u}=(\hat{x}+\hat{y})/\sqrt{2}$. The solid curves represent ideal cases, and the dashed curves represent the best fit to the experimental results.

two-qubit entanglement yet, and the data in Fig. 4 are taken with a single atom at a time loaded to either the q_0 or q_{+1} site while the q_0-resonant rf pulses are applied. Fidelity $\mathcal{F}$ of the rotations, each of which consists of a sequence of unitary transformations on a pure spin state, is simply given by projection of the measured state $|\psi'\rangle$ to the intended state $|\psi_0\rangle$: $\mathcal{F}=|\langle\psi_0|\psi'\rangle|^2$ [17,25]. For the target qubit, $|\psi_0\rangle=R(\hat{x},\pi)R(\hat{v},\theta)|\chi_-\rangle$; and for the nontarget qubit, $|\psi_0\rangle=R(\hat{x},\pi)|\chi_-\rangle$. On the other hand, $|\psi'\rangle$ is written as $\cos\theta'|\chi_0\rangle+\sin\theta' e^{i\phi'}|\chi_1\rangle$, and (θ',ϕ') are obtained from the best fit to the data in Fig. 4. Results from the fitted $|\psi'\rangle$ are shown as the dashed curves. We assume that the final $\pi/2$ pulse and the spin-state detection are perfect, thereby relegating their imperfections to the estimation of $\mathcal{F}$. The results are summarized in Table I. Fidelity of the $R(\hat{u},\pi)$ operation, which involves a jump in ϕ_p at every step, is the lowest. This and other diagnostic measures imply that imperfect rf control is the limiting factor. Because durations of the $\pi/2$ and $R(\hat{v},\theta/2)$ pulses differ by two orders of magnitude, the rf power must change by four orders, straining precision of our rf control. Our simple simulation to find an rf waveform can also be improved by using a method based on optimal control theory to design rf pulses for a specific unitary transformation on a multidimensional Hilbert space [26]. We plan to implement a dual-channel rf system with better optimized waveforms for an experiment on two-qubit gates.

TABLE I. Fidelity of the three gate operations on the target and nontarget qubits. Uncertainties are quoted at the 68% confidence level.

	$R(\hat{x},\pi)$	$R(\hat{x},\pi/2)$	$R(\hat{u},\pi)$
q_0 (target) qubit	0.91 ± 0.05	0.99 ± 0.01	0.88 ± 0.05
q_{+1} (nontarget) qubit	0.93 ± 0.04	0.97 ± 0.04	0.97 ± 0.05

In summary, we have developed an experimental scheme to load a single atom to a specific site and perform a gate operation on a target atom without perturbing coherence of a nearby atom in a 1D lattice when the site separation is only 532 nm. Critical ingredients are magic polarization to enhance spectroscopic resolution without an excessive magnetic field gradient and *in situ* imaging of a Li atom without involving a complicated cooling process, as well as tight control of various experimental parameters. The gate time of ~20 ms is limited by the field gradient. Improvements in coil design and current stability should allow a larger gradient, and hence reduced gate time, without degrading the fidelity. With the capability for a coherent manipulation of individual qubits at our disposal, we plan to entangle adjacent atomic qubits using a blockade by cold collisions in a superlattice. We have constructed a Fabry-Perot cavity in vacuo with resonances at both $\lambda=$ 980 nm and $2\lambda=1960$ nm [27]. For the qubits further apart, the ac Zeeman shift and the off-resonant transition probability decrease rapidly, and our scheme should be applicable to a multiqubit system.

We thank Seokchan Yoon and J. H. Lee for valuable discussions. This work was supported by the National Research Foundation of Korea (Grant No. 2017R1A2B3002543).

*cho@korea.ac.kr

[1] D. Jaksch, H.-J. Briegel, J. I. Cirac, C. W. Gardiner, and P. Zoller, Phys. Rev. Lett. **82**, 1975 (1999).

[2] G. K. Brennen, C. M. Caves, P. S. Jessen, and I. H. Deutsch, Phys. Rev. Lett. **82**, 1060 (1999).
[3] O. Mandel, M. Griner, A. Widera, T. Rom, T. W. Hänsch, and I. Bloch, Nature (London) **425**, 937 (2003).
[4] M. Saffman, J. Phys. B **49**, 202001 (2016).
[5] Y.-Y. Jau, A. M. Hankin, T. Keating, I. H. Deutsch, and G. W. Biedermann, Nat. Phys. **12**, 71 (2016).
[6] H. Levine, A. Keesling, A. Omran, H. Bernien, S. Schwartz, A. S. Zibrov, M. Endres, M. Greiner, V. Vuletic, and M. D. Lukin, Phys. Rev. Lett. **121**, 123603 (2018).
[7] E. A. Goldschmidt, T. Boulier, R. C. Brown, S. B. Koller, J. T. Young, A. V. Gorshkov, S. L. Rolston, and J. V. Porto, Phys. Rev. Lett. **116**, 113001 (2016).
[8] O. Hosten, J. J. Engelsen, R. Krishnakumar, and M. A. Kasevich, Nature (London) **529**, 505 (2016).
[9] R. Raussendorf and H. J. Briegel, Phys. Rev. Lett. **86**, 5188 (2001).
[10] H. J. Briegel, D. E. Browne, W. Dür, R. Raussendorf, and M. Van den Nest, Nat. Phys. **5**, 19 (2009).
[11] D. Schrader, I. Dotsenko, M. Khudaverdyan, Y. Miroshnychenko, A. Rauschenbeutel, and D. Meschede, Phys. Rev. Lett. **93**, 150501 (2004).
[12] M. Karski, L. Förster, J. M. Choi, A. Steffen, N. Belmechri, W. Alt, D. Meschede, and A. Widera, New J. Phys. **12**, 065027 (2010).
[13] A. Derevianko and C. C. Cannon, Phys. Rev. A **70**, 062319 (2004).
[14] H. Kim, S. H Yim, and D. Cho, J. Korean Phys. Soc. **51**, 1279 (2007).
[15] C. Zhang, S. L. Rolston, and S. Das Sarma, Phys. Rev. A **74**, 042316 (2006).
[16] C. Weitenberg, M. Endres, J. F. Sherson, M. Cheneau, P. Schauß, T. Fukuhara, I. Bloch, and S. Kuhr, Nature (London) **471**, 319 (2011).
[17] Y. Wang, X. Zhang, T. A. Corcovilos, A. Kumar, and D. S. Weiss, Phys. Rev. Lett. **115**, 043003 (2015).
[18] Y. Wang, A. Kumar, T-Y Wu, and D. S. Weiss, Science **352**, 1562 (2016).
[19] H. Kim, H. S. Han, and D. Cho, Phys. Rev. Lett. **111**, 243004 (2013).
[20] H. S. Han, S. Yoon, and D. Cho, J. Korean Phys. Soc. **66**, 1675 (2015).
[21] H. S. Han, H. G. Lee, S. Yoon, and D. Cho, J. Phys. B **51**, 155002 (2018).
[22] W. S. Bakr, J. I. Gillen, A. Peng, S. Fölling, and M. Greiner, Nature (London) **462**, 74 (2009).
[23] J. F. Sherson, C. Weitenberg, M. Endres, M. Cheneau, I. Bloch, and S. Kuhr, Nature (London) **467**, 68 (2010).
[24] M. F. Parsons, F. Huber, A. Mazurenko, C. S. Chiu, W. Setiawan, K. Wooley-Brown, S. Blatt, and M. Greiner, Phys. Rev. Lett. **114**, 213002 (2015).
[25] M. D. Bowdrey, D. K. L. Oi, A. J. Short, K. Banaszek, and J. A. Jones, Phys. Lett. A **294**, 258 (2002).
[26] B. E. Anderson, H. Sosa-Martinez, C. A. Riofrio, I. H. Deutsch, and P. S. Jessen, Phys. Rev. Lett. **114**, 240401 (2015).
[27] A Tm-doped fiber laser produces the 1960-nm beam, and the 980-nm beam is to be obtained by doubling its frequency.